

Journal of Materials Chemistry C

Accepted Manuscript



This is an *Accepted Manuscript*, which has been through the Royal Society of Chemistry peer review process and has been accepted for publication.

Accepted Manuscripts are published online shortly after acceptance, before technical editing, formatting and proof reading. Using this free service, authors can make their results available to the community, in citable form, before we publish the edited article. We will replace this *Accepted Manuscript* with the edited and formatted *Advance Article* as soon as it is available.

You can find more information about *Accepted Manuscripts* in the [Information for Authors](#).

Please note that technical editing may introduce minor changes to the text and/or graphics, which may alter content. The journal's standard [Terms & Conditions](#) and the [Ethical guidelines](#) still apply. In no event shall the Royal Society of Chemistry be held responsible for any errors or omissions in this *Accepted Manuscript* or any consequences arising from the use of any information it contains.

Intercalation of coumaric acids into layered rare-earth hydroxide: controllable structure and photoluminescence property

Qingyang Gu, Feifei Su, Lijiao Ma, Shulan Ma,* Genban Sun, Xiaojing Yang

Received (in XXX, XXX) Xth XXXXXXXXX 200X, Accepted Xth XXXXXXXXX 200X

First published on the web Xth XXXXXXXXX 200X

DOI: 10.1039/b000000x

Organic compounds of ortho-coumaric acid (*abbr.* *o*-CMA) and para-coumaric acid (*abbr.* *p*-CMA) are intercalated into the layered rare-earth hydroxide (LRH, R= Eu, Gd) by ion exchange method. The two organics having the same phenolic hydroxyl and carboxyl groups locating different positions demonstrate variant intercalation structures. The CMA anion guests within the LRH gallery indicate monolayered or bi-layered arrangements depending on their own characteristic feature and the deprotonation degree. The combination of *o*-/*p*-CMA molecules with LEuH/LGdH layers generates hybrid materials exhibiting versatile luminescence properties. In solid state, for LEuH layers, the luminescence of layer Eu^{3+} and interlayer *o*-CMA is co-quenched, however, for LGdH layers, green emissions (~520 nm) are observed, both of which are different from the cyan emission (475 nm) of free *o*-CMA anions. When dispersed in formamide (FM), *o*-CMA-LEuH composites exhibit weak luminescence, in sharp contrast to *o*-CMA-LGdH composites displaying green emissions (495-520 nm) with markedly enhanced intensity. The *p*-CMA-LGdH composites display blue emission (457 nm) quite different from the green emission (499 nm) for free *p*-CMA in FM, compared with the unobservable emission within LEuH layers. In addition, co-intercalation of surfactant OS (1-octane sulfonic acid sodium) with *o*-CMA anions into LEuH produces composites showing desirable blue emission or violet emission, due to the change of microenvironment of organic guests. The energy transfer between layer Eu^{3+} and interlayer CMA was proposed to account for the co-quenching or blue shift. This work offers a beneficial approach to fabricate organic-inorganic photofunctional materials with controllable structure and tunable fluorescence property.

1. Introduction

Organic-inorganic hybrid luminescent materials have attracted increasing interest for the novel properties originating from the synergetic interactions of the inclusive components. Layered inorganic materials with two-dimensional (2D) matrices can be readily functionalized *via* intercalation because of their tunable interlayer space and compositions. The incorporation of host matrices and luminescent guests with organized packing modes¹⁻³ can tune the luminescence properties. If the arrangement or loading of luminescent guests can be controlled purposefully within the 2D matrix, the modulation of luminescence would be achieved.^{4, 5} Layered double hydroxides (LDHs) are one type of 2D matrices with positive-charged layers and interlayer counter anions exhibiting a large versatility of applications.^{4, 6-12} Much work involving LDH-chromophore hybrids had been done,¹³⁻¹⁹ however, most of them emphasised on the luminescence property of organic chromophores themselves rather than LDH layers, because these layers are generally not photoactive thus only serving as inorganic matrices for organics. So far, the synergetic effect of organic chromophores and inorganic 2D matrices containing photoactive ions such as Eu^{3+} or Tb^{3+} has not been established. Layered rare earth hydroxides (LRHs), a newly emerging

class of 2D materials structurally similar to LDHs, have attracted increasing attentions of researchers.²⁰⁻²⁶ The lanthanide elements introduced in the host layers can offer multifunctional materials applied in more fields such as luminescence, adsorbents, magnets and catalysis.^{10, 27-29} To date, some studies have focused on the incorporation of organic sensitizers with LRHs to develop new photofunctional materials,³⁰⁻³³ including our work on intercalation of organic compounds into Eu-containing LRHs (LEuH, LYH:Eu and LGdH:Eu).³⁴⁻³⁶ But most of these studies investigated the sensitization or quenching effect of organic compounds on the luminescence of layer ions such as Eu^{3+} and Tb^{3+} . It is noted that if there exists spectra overlap between emission and excitation spectrum of the two interacted components, energy transfer would occur,³⁷ and the synergetic energy transfer effect between photoactive lanthanide ions in the host layer and interlayer organics may bring about fantastic luminescence behaviors, however, there has been a lack of studies focusing on this field, except our recent work on LEuH-chromophore hybrids.³⁸

Coumaric acid is a kind of organic phenolic acids with biological activity, among which the para-coumaric acid (*abbr.* *p*-CMA) has a large number of applications on medicine and agriculture,³⁹⁻⁴¹ and ortho-coumaric acid (*abbr.* *o*-CMA) is one of the best phenolic acids that inhibit intracellular triglyceride and glycerol-3-phosphate dehydrogenase (GPDH)

activity.⁴² The *o*-CMA and *p*-CMA are structurally similar with the same hydroxyl and carboxyl groups but the two groups locate at different positions, thus possibly giving rise to versatile intercalation structure and varied luminescence properties. In this work, we introduce the *o*-CMA and *p*-CMA (Scheme S1) into the gallery of LEuH/LGdH, to investigate the intercalation structure and luminescence property. We demonstrate here, distinct green emission observable for *o*-CMA-LGdH composites, while co-quenching effect for *o*-CMA-LEuH composites. The *p*-CMA-LGdH display blue emission, in contrast to the weak emission for *p*-CMA-LEuH. The addition of an anionic surfactant of 1-octane sulfonic acid sodium (OS) leads to marked blue emissions of composites. The present work provides important insight for preparation of organic-inorganic hybrid materials with controllable structure and tunable optical property.

2. Experimental section

2.1 Preparation of NO₃-LEuH precursor.

The NO₃-LEuH was synthesized *via* a hydrothermal method as previously reported.^{34, 35} An aqueous solution containing Eu(NO₃)₃·6H₂O (1 mmol), hexamethylenetetramine (HMT, 1 mmol), NaNO₃ (13 mmol), and deionized water (80 mL) was heated at 90 °C for 12 h in a Teflon-autoclave. After the product was filtered, washed, and vacuum-dried (40 °C for 24 h), the NO₃-LEuH precipitate was obtained.

The preparation procedure for NO₃-LGdH is similar to that of NO₃-LEuH, using Gd(NO₃)₃·6H₂O to substitute for Eu(NO₃)₃·6H₂O.

2.2 Syntheses of CMA-LRH composites.

The ion-exchange reactions between NO₃⁻ and the organic anions were processed at 70 °C in a Teflon-autoclave. Firstly, 0.207 g (1.26 mmol) *o*/*p*-CMA and 0.054 g/0.108 g (1.26 mmol/2.52 mmol) NaOH (corresponding to 1:1 or 2:1 molar ratio of NaOH to *o*/*p*-CMA) were mixed to the obtained solutions (80 ml) for deprotonation of the organic species. The NO₃-LEuH or NO₃-LGdH powder (~0.1 g) was dispersed into the above solutions, then reacted at 70 °C for 24 h in a Teflon-autoclave. The resulting precipitates were collected by filtration, washed with deionized water, and vacuum-dried at 40 °C for 24 h. The as-prepared composites are noted as CMA-LRH-*x*, in which *x* is the molar ratio of NaOH to CMA, for example *o*-CMA-LEuH-1:2 represents the molar ratio of *o*-CMA to NaOH is 1:2.

2.3 Syntheses of OS-CMA-LEuH composites.

Firstly, 0.207 g (1.26 mmol) CMA and 0.054 g (1.26 mmol) NaOH and 0.273 g (1.26 mmol) OS were mixed to obtain solutions (80 ml). The NO₃-LEuH powder (0.1 g) was dispersed into the above solutions, then reacted at 70 °C for 24 h in a Teflon-autoclave. The resulting precipitates were collected by filtration, washed with deionized water, and vacuum-dried at 40 °C for 24 h. The as-prepared composite is noted as OS-CMA-LEuH-1:1.

2.4 Luminescence testing conditions for samples.

0.025 g composites were dispersed into 10 mL FM by mechanical shaking for 24 h to form colloidal suspensions to conduct the luminescence measurements. For organics of *o*-CMA and *p*-CMA, NaOH is added to make them deprotonated to make them deprotonated, and when dissolved in FM, solutions for them were obtained.

2.5 Characterization Techniques.

The powder X-ray diffraction (XRD) patterns were collected by using a Phillips X'pert Pro MPD diffractometer with Cu-K α radiation at room temperature, with a step size of 0.0167 °, scan time of 15 seconds per step, and 2θ ranging from 4.5 to 70 °. The generator setting was 40 kV and 40 mA. For the small degrees, the XRD patterns were measured at room temperature with step size of 0.008 °, scan time of 30 seconds per step. Fourier transformed infrared (FT-IR) spectra of the samples were recorded on a Nicolet-360 Fourier-Transform infrared spectrometer by the KBr method. Scanning electron microscope (SEM) observations were carried out by using a Hitachi S-4800 microscope at 5.0 kV. Luminescence spectra were obtained on a Cary Eclipse spectrofluorimeter and Shimadzu RF-5301PC spectrofluorimeter.

The metal ion contents were determined by inductively coupled plasma atomic emission spectroscopy (ICP-AES, Jarrel-ASH, ICAP-9000) after the solid products were dissolved in a 0.1 M HNO₃. C, H and N contents were determined by using an Elementar vario EL elemental analyzer. The chemical formula of the products were determined based on the results of ICP and CHN analyses.

3. Results and Discussion

3.1 Structure analyses of the as-prepared composites.

Fig. 1 shows the XRD patterns of NO₃-LEuH/LGdH precursors and the composites. As shown in Fig. 1, the basal spacing (d_{basal}) of 0.83/0.82 nm for LEuH/LGdH is the same as we previously reported.^{34, 35} The *o*-CMA-LEuH-1:1 composite (Fig. 1A-b) has a d_{basal} value of 2.12 nm, corresponding to a series of (00*l*) reflections at 2.12, 1.07, 0.72, and 0.54 nm. When the molar ratio of *o*-CMA to NaOH is increased to be 1:2, the XRD pattern of the obtained composite *o*-CMA-LEuH-1:2 (Fig. 1A-c) shows a d_{basal} value of 1.24 nm, and there is no reflection in the range of small angle. On the basis of the layer thickness of LRH (0.65 nm),³⁴ the gallery height for *o*-CMA-LEuH-1:1 is ca. 1.47 nm (= 2.12-0.65), which corresponds to an alternating bi-layered tilted arrangement (Scheme 1b), considering the *o*-CMA height of 0.82 nm with a size of 0.82×0.46×0.31 nm. The gallery height for *o*-CMA-LEuH-1:2 is ca. 0.59 nm (= 1.24-0.65), so the *o*-CMA molecules may be placed horizontally in the interlayer, corresponding to a monolayer and horizontal arrangement (Scheme 1d). The *o*-CMA-LEuH-1:2 relate to duple NaOH would have a stronger affinity of the gallery anions to the layer, thus leading to a decreased d_{basal} .

For *p*-CMA, at an equimolar ratio of *p*-CMA to NaOH (*p*-CMA-LEuH-1:1), although a new peak at 1.25 nm appears (Fig. 1A-d), the reflection of NO₃-LEuH precursor at 0.82 nm is dominant, suggesting the exchange reaction is not complete.

The 1.25 nm peak means an intercalated phase of 2.4-2.5 nm d_{basal} (the 1.25 nm peak may be its (004) inflection) may be present, but its amount is too little that this phase cannot be detected by XRD. As shown in the XRD patterns (Fig. S1, ESI†), the changed reaction conditions such as elongated time or higher temperature did not give obvious improvement for the exchange degree. The variant intercalation results of *o*-CMA and *p*-CMA under the same reaction condition show their structure nature plays a key role for the intercalation. The *o*-CMA and *p*-CMA have different structural characteristics though they have the similar groups. The *o*-CMA molecules can form a ring type *via* intramolecular hydrogen bonds, while *p*-CMA would only form intermolecular hydrogen bonds. Compared with *o*-CMA, the stronger intermolecular hydrogen bonding interactions in *p*-CMA molecules may give rise to a weaker reaction affinity with the LRH layers.

When the molar ratio of NaOH to *p*-CMA and is increased to 2:1, the obtained composite *p*-CMA-LEuH-1:2 (Fig. 1A-e) reveals a d_{basal} value of 1.48 nm, with series of (00*l*) reflections at 1.48, 0.77, 0.52 and 0.38 nm. Considering the *p*-CMA size of $\sim 0.84 \times 0.44 \times 0.31$ nm, the gallery height of ca. 0.83 nm (= 1.48-0.65) for *p*-CMA-LEuH-1:2 corresponds to a monolayer vertical arrangement (Scheme 1e). In contrast to the horizontal arrangement of *o*-CMA with the same NaOH/CMA molar ratio of 2:1 above mentioned, the vertical orientation for *p*-CMA in the interlayer is probably due to the two negatively-charged -COO⁻ and -O⁻ groups locating on the opposite positions of the molecule. One of the two groups may be anchored to each face of the LRH layer, thus favoring the vertical orientation, as found in our reported LDH composites.⁴³ Most of the XRD patterns of CMA-LGdH composites (Fig. 1B) are similar to those of LEuH composites, except the *p*-CMA-LGdH-1:1 (Fig. 1B-d) with a 1.42 nm d_{basal} , which demonstrates that different LRH layers sometimes produce slightly various intercalation structure.

In addition, after OS is added, the obtained composites exhibit different structures (Scheme 1c and 1f). As shown in Fig. 1A-f,f', OS-*o*-CMA-LEuH-1:1 is a pure phase showing a d_{basal} of 2.12 nm, with a series of (00*l*) reflections at 2.12, 1.06, 0.72 and 0.53 nm. However, OS-*p*-CMA-LRH (Fig. 1A-g,g') reveals a mixture of three phases with three d_{basal} values of 2.28, 1.98 and 1.30 nm. The much enlarged d_{basal} for the composites demonstrate the long chained OS anions mainly support the LRH gallery. The ring type structure for *o*-CMA formed by intramolecular hydrogen bonds may help give a pure intercalated phase, while the *p*-CMA with much freedom for structural twist would bring about the varied intercalated phases especially in the presence of the surfactant OS.

Based on ICP, CHN analyses and charge balance considerations, the compositions of the LEuH precursor and the as-prepared composites were estimated as shown in Table 1. The chemical formula of the NO₃-LEuH/LGdH precursors are determined as Eu(OH)_{2.41}(NO₃)_{0.49}(CO₃)_{0.05}·0.8H₂O and Gd(OH)_{2.42}(NO₃)_{0.42}(CO₃)_{0.08}·0.9H₂O. In the composites, the contents of CMA in CMA-LRH-1:1 is two folds of that in CMA-LRH-1:2, which is in agreement with the valences of the CMA relate to the equimolar and duple NaOH. In *p*-CMA-

LEuH-1:1, the significant amount of NO₃⁻ shows the incomplete ion-exchange, coincident with the XRD results discussed above. In addition, there are some CO₃²⁻ found in the compositions. CO₃²⁻ in the precursors should originate from the decomposition of the hexamethylene tetramine (HMT) during the hydrothermal reaction, while the CO₃²⁻ in the composites would result from the incomplete exchange of the introduced organic species and the starting anions.

3.2 IR and morphology of the as-prepared composites.

Fig. 2 show the FT-IR spectra of the precursors and composites. For NO₃-LEuH/LGdH (Fig. 2a,b), the sharp and strong absorption peak at 1384 cm⁻¹ is characteristic of ν₃ vibration mode of free NO₃⁻.⁴⁴ For *o*-CMA (Fig. 2c), the bands at 1668 and 1461 cm⁻¹ are ascribed to ν_{as} and ν_s vibrations of -COOH group. The band at 1617 cm⁻¹ is the stretching vibration of the -C=C band. After forming composites, for *o*-CMA-LEuH/LGdH-1:1 (Fig. 2e,i), the bands at 1520/1522 and 1423/1420 cm⁻¹ are assigned to the ν_{as} and ν_s vibrations of deprotonated -COO⁻ group, and the deprotonation of -COOH results in the red shift. The bands at 1633/1630 cm⁻¹ are the stretching vibration of -C=C band. For *o*-CMA-LEuH/LGdH-1:2 (Fig. 2f,j), the ν_{as} and ν_s vibrations of -COO⁻ appear at 1526/1522 and 1384 /1385 cm⁻¹, respectively, and the bands at 1623/1630 cm⁻¹ are related to the C=C vibrations.

For *p*-CMA (Fig. 2d), the ν_{as} and ν_s vibrations of -COOH appear at 1672 and 1448 cm⁻¹, the C=C vibration is present at 1601 cm⁻¹, as well as the vibration of benzene ring at 1512 cm⁻¹. After intercalation, the ν_{as} and ν_s vibrations of -COO⁻ occur at 1607/1598 cm⁻¹ and 1384/1420 cm⁻¹ for *p*-CMA-LEuH/LGdH-1:1 (Fig. 2g, k). The ν_{as} and ν_s vibrations of -COO⁻ occur at 1593/1598 cm⁻¹ and 1384/1385 cm⁻¹ for *o*-CMA-LEuH/LGdH-1:2 (Fig. 2h, l). The vibrations for C=C appear at around 1630 cm⁻¹ and that for benzene ring are around 1510 cm⁻¹ in the composites. The peaks ~ 600 cm⁻¹ ascribed to Eu/Gd-O vibrations³⁴ also verify the formation of the layered composites.

Fig. 3 presents typical SEM images of the layered materials. NO₃-LEuH precursor (Fig. 3a,a') is mainly crystallized into elongated hexahedron platelets with edge lengths up to $\sim 5 \times 20$ μm². Most of the composites (Fig. 3b-e') remain the hexagonal plate-like morphology, and some grow into columnar or flower-like aggregates. These morphologies were observed in our precious work.^{34, 35}

3.3 Luminescence property of composites in solid state.

Fig. 4 show the powder excitation and emission spectra of LEuH, *o*-CMA and *o*-CMA-LRH composites. The excitation spectra of LEuH (Fig. 4A-a) is monitored from the intra-4f⁶ emission (⁵D₀-⁷F₂, λ_{em} = 614 nm) of Eu³⁺, and the sharp peak at 395 nm is due to intra-ionic transition ⁷F₀-⁵L₆ of Eu³⁺. The emission spectrum of NO₃-LEuH (Fig. 4B-a) is measured using the excitation wavelength of 395 nm of Eu³⁺. Typical emission peaks are observed at 580, 589/595, 613, 654, and 698 nm, assigned to ⁵D₀-⁷F_{*J*} (*J* = 0, 1, 2, 3, 4) radiative-relaxational transitions of Eu³⁺.⁴⁵ For the *o*-CMA-Na in solid state, there exists an excitation peak at 420 nm (Fig. 4A-b),

corresponding to the cyan emission peak at 475 nm (Fig. 4B-b). However, in *o*-CMA-LEuH composites, neither emissions of layer Eu³⁺ nor emission of CMA is observable (Fig. 4B-c,d), revealing a co-quenching phenomenon, in well agreement with the unobserved excitation (Fig. 4A-c).

For composite *o*-CMA/NaOH-1:1, the *o*-CMA has one -OH group without deprotonation, so the quenching effect may be ascribed to the significant nonradiative relaxation channels provided by the high-energy vibration of -OH group.^{46,47} For CMA:NaOH ratio of 1:2, the -OH of CMA would also be deprotonated, thus the alike quenching suggests should be ascribed to an energy transfer existing in the system. For the energy transferring process, a suitable interaction between absorption and emission centers would exist.²¹ There is certain overlap for the excitations for Eu³⁺ (250-550 nm, Fig. 4A-a) and emission of *o*-CMA-Na (400-600 nm, Fig. 4B-b), which mean that there is energy transfer between the layer Eu³⁺ and CMA anions causing the co-quenching. Meanwhile, the high-energy vibration of -OH of *o*-CMA anions will also compete the provided energy to produce nonradiative relaxation channels, thus accelerating the co-quenching. Similar co-quenching phenomenon for LEuH-HPTS composite was also found in our previous work.³⁸

To investigate the function of other layer ions, LGdH layer is used to check the luminescence behavior. Fig. 4C showed the powder excitation spectra of *o*-CMA-LGdH composites, demonstrating obvious excitations at 429 nm for the *o*-CMA-LGdH-1:1 and 408 nm for *o*-CMA-LGdH-1:2. Under the excitation at these above wavelengths, obvious green emission at 523 nm for *o*-CMA-LGdH-1:1 and 516 nm for *o*-CMA-LGdH-1:2 are observable (Fig. 4D). The emissions within LGdH layers reflect mainly the luminescence of *o*-CMA, for which the emission shifts from cyan to green originate from the changed microenvironment of *o*-CMA provided by the LGdH layers. In addition, the emission intensity for *o*-CMA-LGdH-1:1 is stronger than that of *o*-CMA-LGdH-1:2, attributed to the increscent emission centers and absorption cross section of *o*-CMA in *o*-CMA-LGdH-1:1. This is in agreement with the compositions of the composites as shown in Table 1. Herein, the observable emission of organics indicates the LGdH layers play an important role in preventing intermolecular interactions of organics and their aggregation within host layers, as acted by LDH layers.⁴⁸ The rigid and enclosed environment provided by the LRH layers confines the internal mobility and flexibility of the interlayer guests, especilaly the CMA molecules with near-plane configuration, thus promoting the CMA emission. Gd³⁺ can increase the absorbance of the host and the interactions between host and guests, as found in the previous work for L-LTbH:Gd (L is a carboxylic acid sensitizer), the vast majority of UV absorption was initially performed by the LTbH:Gd host rather than by the sensitizer L.³⁰ In contrast, the LEuH layer here exhibits different function such as the energy transfer contributing to co-quenching.

3.4 Luminescence of *o*-CMA-LRH composites in FM.

The luminescent property of *o*-CMA-Na solution and the colloidal suspensions of the composites dispersed in FM were

investigated systematically. The emission spectrum for all the composites was obtained under 365 nm the same as the normal UV light. The luminescence of *o*-CMA-LEuH composites in FM cannot be observed (Fig. 5A-a,b), while the LGdH composites display bluish green (496 nm) for *o*-CMA-LGdH-1:1 and green emission (517 nm) for *o*-CMA-LGdH-1:2 (Fig. 5A-c,d). The x and y emission color coordinates of *o*-CMA-LGdH composites in the 1931 CIE chromaticity diagram is depicted in Fig. 5A'. Their emission color is in agreement with the emissions.

For the OS added composite of OS-*o*-CMA-LEuH-1:1, we measured its luminescence when dispersed it in FM. Under the excitation wavelength of 365 nm, OS-*o*-CMA-LEuH-1:1 (Fig. 5B-a) displays blue emission at 464 nm, forming distinct contrast to the green light of the LGdH composites and free *o*-CMA anions in FM (Fig. 5B-b). Fig. 5B' shows the CIE of the OS-*o*-CMA-LRH composite, which is in agreement with the emission band of the corresponding composite. Here the introduction of OS brings about the change of the emission position and intensity, demonstrating the important function OS acts. As we know, surfactants can alter the aggregation of photoactive species.⁴⁹ The surfactant (here is OS) would dilute/isolate CMA anions so as to prevent their aggregation that weakens the luminescence.⁵⁰⁻⁵³ In present system, the OS serving as an anionic surfactant affects not only the emission intensity but also the peak position, in comparasion with the results reported by Ramon et al.⁵⁴ The altered emission position may be owing to a microenvironment change of *o*-CMA anions when OS interacted with *o*-CMA and the positive-charged LEuH layers. Some supramolecular structures *via* intermolecular interactions between rigid CMA and flexible OS anions may also be formed thus causing the change of the molecular configuration and steric arrangement of *o*-CMA as found in other compounds,^{53,55} so as to alter the energy levels of *o*-CMA further the luminescence behaviors. In addition, the surfactants play a key role in the delamination of the composites. As known, anionic surfactants such as sodium dodecyl sulfate (DS) with long aliphatic chains were conducive to perform the delamination of LRHs.^{45,56} In our recent work, we found the surfactant OS with short-chains can also help achieve the one-step delamination of the composites.³⁸ Now the same delamination phenomenon happens. During this case, the delaminated LEuH nanosheets with high freedom could combine with the *o*-CMA anions as close as possible *via* electrostatic interactions, thus generating the distinct emission results.

3.5 Luminescence of *p*-CMA-LRH composites in FM.

The luminescent property of *p*-CMA-LRH composites in FM were investigated under the excitation of 365 nm (Fig. 6A). The *p*-CMA anions in FM solution displays green emission at 499 nm, while the *p*-CMA-LGdH composites present blue emission at 457 nm, meanwhile, the *p*-CMA-LEuH composites showed no emissions. In the case with OS addition, the obtained composite of OS-*p*-CMA-LEuH-1:1 gives violet emission around 422 nm (Fig. 6B). The colors in CIE chromaticity diagram are in agreement with the emission peaks (Fig. 6A', B'). The reason for the enhanced emission

intensity and the changed peak position in the presence of OS may be the same as that discussed for the OS-*o*-CMA-LEuH composite. In both of the two cases for *o*-CMA and *p*-CMA, the OS added composites revealed evident emission enhancement and blue shift, which may result from the change of the microenvironments of the photoactive CMA anions. As shown in the excitation spectra (Fig. S2, ESI†) of the composites before and after OS addition, the different excitation wavelengths mean varied chemical environment of CMA, which contributes to the different luminescence behaviors.

3.6 Luminescence mechanism of the composites in solid state and colloidal state.

As discussed above, in solid state, for *o*-CMA-LGdH composites, the confinement effect of the host LGdH layer makes the *o*-CMA luminescence observable. However, for the *o*-CMA-LEuH composites, certain energy transfer between layer Eu³⁺ ion and CMA anions results in the co-quenching. The overlap between the excitation and emissions of Eu³⁺ and *o*-CMA may account for the mutual energy transfer. Meanwhile, the high-energy vibration of -OH of *o*-CMA anions will also compete the provided energy to produce nonradiative relaxation channels, thus accelerating the co-quenching. In FM, the host layers are present at a delaminated state and the positively-charged LRH layers would provide a unique arrangement and microenvironment for CMA anions that adhere to the LRH layers through electrostatic interactions. Compared with that in solid state, the confinement effect by LRH layers for CMA under the delaminated state is markedly weakened and the electrostatic interaction among them becomes dominant. All these contribute to the different luminescence behaviors. In addition, the varied layer ions such as Eu³⁺ and Gd³⁺ give rise to different luminescence behaviors though at the same condition, which highlights the function of host layer ions. The LGdH layer may help adsorb the energy and function as a host bridge that transfer energy to CMA, while the LEuH layer might competitively adsorb the energy thus weakening the emission of CMA.

4. Conclusions

In summary, the *o*-CMA and *p*-CMA are intercalated into the LRHs (R = Eu, Gd) by ion exchange to form versatile intercalation structures. The CMA anions within the interlayer adopt monolayered or bi-layered arrangements depending on the degree of deprotonation following the amount of NaOH added. The composites exhibiting tunable fluorescence behaviors depending on the state and layer ion type. In solid state, layer confinement effect and energy transfer result in co-quenching for Eu³⁺ and CMA emissions, while for LGdH layers, the composites display mainly the luminescence of CMA. In FM, LEuH layers still exhibit no luminescence, while LGdH layers present green emission for *o*-CMA-LGdH and blue emission for *p*-CMA-LGdH, showing enhanced or different emission from free CMA anions. The addition of surfactant OS helps the complete delamination of the composites, which leads to emissions with large blue shift.

Thus, the confinement effect of LGdH layer enhances emissions of interlayer CMA emission, the energy transfer between layer Eu³⁺ and CMA results in the co-quenching. The introduction of surfactant OS causes the blue shift of emissions for LEuH layers, which arises from the change of microenvironment of CMA in completely delaminated state. This study is expected to open a new field of LRHs for fabricating color-tuning inorganic-organic luminous materials via adjusting the structure or microenvironment of photoactive organics.

Acknowledgments.

This work is supported by the National Science Foundations of China 21271028, 51272030 and 21271001.

Notes and references

Beijing Key Laboratory of Energy Conversion and Storage Materials, College of Chemistry, Beijing Normal University, Beijing 100875, China.

Fax: 86 10 5880 2075; Tel: 86 10 5880 7524; E-mail:

mashulan@bnu.edu.cn

† Electronic Supplementary Information (ESI) available: structural diagram of organic species of *o*-CMA and *p*-CMA, XRD patterns of *p*-CMA-LEuH-1:1 composite prepared at different reaction conditions, excitation spectra of composites in FM. See DOI: 10.1039/b000000x/.

1. V. M. Agranovich, Y. N. Gartstein and M. Litinskaya, *Chem. Rev.*, 2011, **111**, 5179.
2. N. Yanai, K. Kitayama, Y. Hijikata, H. Sato, R. Matsuda, Y. Kubota, M. Takata, M. Mizuno, T. Uemura and S. Kitagawa, *Nat. Mater.*, 2011, **10**, 787.
3. J. C. Yu, Y. J. Cui, H. Xu, Y. Yang, Z. Y. Wang, B. L. Chen and G. D. Qian, *Nat. Commun.*, 2013, **4**, 2719.
4. D. P. Yan, J. Lu, J. Ma, M. Wei, D. G. Evans and X. Duan, *Angew. Chem. Int. Edit.*, 2011, **50**, 720.
5. C. Seebacher, J. Rau, F. W. Deeg, C. Brauchle, S. Altmair, R. Jager and P. Behrens, *Adv. Mater.*, 2001, **13**, 1374.
6. S. L. Ma, J. Wang, L. Du, C. H. Fan, Y. H. Sun, G. B. Sun and X. J. Yang, *Eur. J. Inorg. Chem.*, 2013, 1363.
7. S. L. Ma, C. H. Fan, L. Du, G. L. Huang, X. J. Yang, W. P. Tang, Y. Makita and K. Ooi, *Chem. Mater.*, 2009, **21**, 3602.
8. X. Y. Xue, Q. Y. Gu, G. H. Pan, J. Liang, G. L. Huang, G. B. Sun, S. L. Ma and X. J. Yang, *Inorg. Chem.*, 2014, **53**, 1521.
9. S. L. Ma, Q. M. Chen, H. Li, P. L. Wang, S. M. Islam, Q. Y. Gu, X. J. Yang and M. G. Kanatzidis, *J. Mater. Chem. A*, 2014, **2**, 10280.
10. F. Geng, R. Ma and T. Sasaki, *Acc. Chem. Res.*, 2010, **43**, 1177.
11. S. L. Ma, Y. Shim, S. M. Islam, K. S. Subrahmanyam, P. L. Wang, H. Li, S. C. Wang, X. J. Yang and M. G. Kanatzidis, *Chem. Mater.*, 2014, **26**, 5004.
12. S. L. Ma, S. M. Islam, Y. Shim, Q. Y. Gu, P. L. Wang, H. Li, G. B. Sun, X. J. Yang and M. G. Kanatzidis, *Chem. Mater.*, 2014, **26**, 7114.
13. B. Johann, B. Peter, S. Markus and L. Heinz, *Adv. Funct. Mater.*, 2003, **13**, 241.
14. D. P. Yan, J. Lu, J. Ma, S. Qin, M. Wei, D. G. Evans and X. Duan, *Angew. Chem. Int. Ed.*, 2011, **50**, 7037.
15. Z. L. Wang, Z. H. Kang, E. B. Wang, Z. M. Su and L. Xu, *Inorg. Chem.*, 2006, **45**, 4364.
16. S. L. Dang, D. P. Yan and J. Lu, *J. Solid State Chem.*, 2012, **185**, 219.
17. W. J. Guan, J. Lu, W. J. Zhou and C. Lu, *Chem. Commun.*, 2014, **50**, 11895.

18. D. P. Yan, J. Lu, M. Wei, D. G. Evans and X. Duan, *J. Phys. Chem. B.*, 2009, **113**, 1381.
19. D. P. Yan, J. Lu, M. Wei, S. Qin, L. Chen, S. Zhang, D. G. Evans and X. Duan, *Adv. Funct. Mater.*, 2011, **21**, 2497.
20. F. Gandara, J. Perles, N. Snejkovic, M. Iglesias, B. Gomez-Lor, E. Gutierrez-Puebla and M. A. Monge, *Angew. Chem. Int. Edit.*, 2006, **45**, 7998.
21. P. Gunawan and R. Xu, *J. Phys. Chem. C.*, 2009, **113**, 17206.
22. F. X. Geng, H. Xin, Y. Matsushita, R. Ma, M. Tanaka, F. Izumi, N. Iyi and T. Sasaki, *Chem. Eur. J.*, 2008, **14**, 9255.
23. J. B. Liang, R. Ma, F. X. Geng, Y. Ebina and T. Sasaki, *Chem. Mater.*, 2010, **22**, 6001.
24. F. Geng, Y. Matsushita, R. Ma, H. Xin, M. Tanaka, N. Iyi and T. Sasaki, *Inorg. Chem.*, 2009, **48**, 6724.
25. F. Geng, Y. Matsushita, R. Ma, H. Xin, M. Tanaka, F. Izumi, N. Iyi and T. Sasaki, *J. Am. Chem. Soc.*, 2008, **130**, 16344.
26. Y. S. Zhao, J. G. Li, M. X. Guo and X. J. Yang, *J. Mater. Chem. C.*, 2013, **1**, 3584.
27. J. B. Liang, R. Z. Ma and T. Sasaki, *Dalton Trans.*, 2014, **43**, 10355.
28. Q. Zhu, J. G. Li, X. D. Li, X. D. Sun, Y. Qi, M. Y. Zhu and Y. Sakka, *Sci. Technol. Adv. Mat.*, 2014, **15**, 014203.
29. H. Kim, B. I. Lee and S. H. Byeon, *Chem. Commun.*, 2015, **51**, 725.
30. L. Liu, Q. Wang, C. Gao, H. Chen, W. Liu and Y. Tang, *J. Phys. Chem. C.*, 2014, **118**, 14511.
31. X. R. Gao, M. Hu, L. X. Lei, D. O'Hare, C. Markland, Y. M. Sun and S. Faulkner, *Chem Commun.*, 2011, **47**, 2104.
32. L.-L. Liu, Q. Wang, D. Xia, T.-T. Shen, M.-H. Yu, W.-S. Liu and Y. Tang, *Chin. Chem. Lett.*, 2013, **24**, 93.
33. M. Watanabe and S. Fujihara, *J. Solid State Chem.*, 2014, **210**, 130.
34. Q. Y. Gu, Y. H. Sun, N. K. i. Chu, S. L. Ma, Z. Q. Jia and X. J. Yang, *Eur. J. Inorg. Chem.*, 2012, **2012**, 4407.
35. Q. Y. Gu, N. K. Chu, G. H. Pan, G. B. Sun, S. L. Ma and X. J. Yang, *Eur. J. Inorg. Chem.*, 2014, **3**, 559.
36. W. L. Li, Q. Y. Gu, F. F. Su, Y. H. Sun, G. B. Sun, S. L. Ma and X. J. Yang, *Inorg. Chem.*, 2013, **52**, 14010.
37. M. Shang, C. Li and J. Lin, *Chem. Soc. Rev.*, 2014, **43**, 1372.
38. Q. Y. Gu, F. F. Su, S. L. Ma, G. Sun, B. and X. J. Yang, *Chem. Commun.*, 2015, **51**, 2514.
39. T. Wallerath, H. G. Li, U. Godtel-Ambrust, P. M. Schwarz and U. Forstermann, *Nitric Oxide-Biol. Ch.*, 2005, **12**, 97.
40. L. R. Ferguson, S. Zhu and P. J. Harris, *Mol. Nutr. Food Res.*, 2005, **49**, 585.
41. Y. L. Lai and M. Yamaguchi, *Mol. Cell. Biochem.*, 2006, **292**, 45.
42. C.-L. Hsu and G.-C. Yen, *J. Agric. Food. Chem.*, 2007, **55**, 8404.
43. F. X. Geng, Y. Matsushita, R. Z. Ma, H. Xin, M. Tanaka, N. Iyi and T. Sasaki, *Inorg. Chem.* 2009, **48**, 6724.
44. Q. Y. Gu, G. H. Pan, T. Ma, G. L. Huang, G. B. Sun, S. L. Ma and X. J. Yang, *Mater. Res. Bull.*, 2014, **53**, 234.
45. L. F. Hu, R. Ma, T. C. Ozawa and T. Sasaki, *Inorg. Chem.*, 2010, **49**, 2960.
46. T. C. Ozawa, K. Fukuda, K. Akatsuka, Y. Ebina and T. Sasaki, *Chem. Mater.*, 2007, **19**, 6575.
47. Y. Matsumoto, U. Unal, Y. Kimura, S. Ohashi and K. Izawa, *J. Phys. Chem. B.*, 2005, **109**, 12748.
48. S. L. Dang, D. P. Yan and J. Lu, *J. Solid State Chem.*, 2012, **185**, 219.
49. M. Ogawa and K. Kuroda, *Chem. Rev.*, 1995, **95**, 399.
50. M. D. Curtis, J. Cao and J. W. Kampf, *J. Am. Chem. Soc.*, 2004, **126**, 4318.
51. J. Dong, K. M. Solntsev and L. M. Tolbert, *J. Am. Chem. Soc.*, 2009, **131**, 662.
52. M. S. Kwon, J. Gierschner, S. J. Yoon and S. Y. Park, *Adv. Mater.*, 2012, **24**, 5487.
53. J. B. Zhang, B. Xu, J. L. Chen, S. Q. Ma, Y. J. Dong, L. J. Wang, B. Li, L. Ye and W. J. Tian, *Adv. Mater.*, 2014, **26**, 739.
54. B. R. Ramon and E. Joan, *J. Phys. Chem. B.*, 2009, **113**, 1972.
55. A. D. Shao, Z. Q. Guo, S. J. Zhu, S. Q. Zhu, P. Shi, H. Tian and W. H. Zhu, *Chem. Sci.*, 2014, **5**, 1383.
56. Y. S. Zhao, J. G. Li, M. X. Guo and X. J. Yang, *J. Mater. Chem. C.*, 2013, **1**, 3584.

Table 1. Chemical compositions for LEuH/LGdH precursor and the composites.

Samples	Chemical formula	Wt %, Found (Calcd.)			
		Eu/Gd	C	H	N
NO ₃ -LEuH	Eu(OH) _{2.41} (NO ₃) _{0.49} (CO ₃) _{0.05} 0.8H ₂ O	62.00 (62.50)	0.27 (0.25)	1.63 (1.73)	2.81 (2.88)
<i>o</i> -CMA-LEuH-1:1	Eu(OH) _{2.41} (C ₉ H ₇ O ₃) _{0.59} (C ₉ H ₈ O ₃) _{0.02} 0.8H ₂ O	50.60 (49.33)	22.00 (20.68)	2.74 (2.67)	-
<i>o</i> -CMA-LEuH-1:2	Eu(OH) _{2.41} (C ₉ H ₆ O ₃) _{0.265} (CO ₃) _{0.03} 1.0H ₂ O	60.30 (59.52)	10.89 (11.21)	2.48 (2.33)	-
<i>p</i> -CMA-LEuH-1:1	Eu(OH) _{2.41} (C ₉ H ₇ O ₃) _{0.48} (C ₉ H ₈ O ₃) _{0.08} (NO ₃) _{0.11} 1.0H ₂ O	49.41 (49.24)	17.70 (16.81)	2.75 (2.49)	0.55 (0.50)
<i>p</i> -CMA-LEuH-1:2	Eu(OH) _{2.40} (C ₉ H ₆ O ₃) _{0.30} 1.33H ₂ O	58.25 (57.29)	12.56 (12.14)	2.68 (2.59)	-
NO ₃ -LGdH	Gd(OH) _{2.42} (NO ₃) _{0.42} (CO ₃) _{0.08} 0.95H ₂ O	64.04 (63.82)	0.42 (0.39)	1.92 (1.78)	2.40 (2.39)
<i>o</i> -CMA-LGdH-1:1	Gd(OH) _{2.42} (C ₉ H ₇ O ₃) _{0.575} (C ₉ H ₈ O ₃) _{0.066} (NO ₃) _{0.005} 1.1H ₂ O	47.92 (48.63)	20.11 (19.22)	2.64 (2.68)	0.02 (0.02)
<i>o</i> -CMA-LGdH-1:2	Gd(OH) _{2.42} (C ₉ H ₆ O ₃) _{0.26} (NO ₃) _{0.0017} (CO ₃) _{0.05} 0.6H ₂ O	62.88 (62.11)	9.79 (10.20)	2.24 (2.05)	0.01 (0.01)
<i>p</i> -CMA-LGdH-1:1	Gd(OH) _{2.42} (C ₉ H ₇ O ₃) _{0.56} (NO ₃) _{0.023} 0.88H ₂ O	50.14 (51.24)	18.88 (19.68)	2.53 (2.64)	0.10 (0.10)
<i>p</i> -CMA-LGdH-1:2	Gd(OH) _{2.42} (C ₉ H ₆ O ₃) _{0.26} (NO ₃) _{0.004} (CO ₃) _{0.03} 0.7H ₂ O	61.60 (61.29)	10.17 (10.87)	2.23 (2.14)	0.02 (0.02)

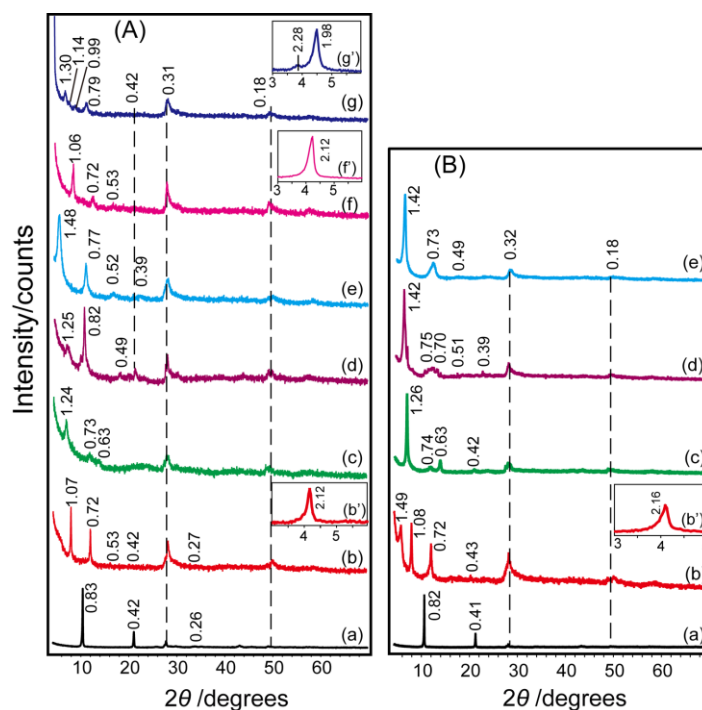


Fig. 1 (A) Powder XRD patterns of precursor $\text{NO}_3\text{-LEuH}$ (a), composites $o\text{-CMA-LEuH-1:1}$ (b,b'), $o\text{-CMA-LEuH-1:2}$ (c), $p\text{-CMA-LEuH-1:1}$ (d), $p\text{-CMA-LEuH-1:2}$ (e), $\text{OS-}o\text{-CMA-LEuH-1:1}$ (f,f'), $\text{OS-}p\text{-CMA-LEuH-1:1}$ (g,g'). (B) XRD patterns of precursor $\text{NO}_3\text{-LGdH}$ (a), composites $o\text{-CMA-LGdH-1:1}$ (b, b'), $o\text{-CMA-LGdH-1:2}$ (c), $p\text{-CMA-LGdH-1:1}$ (d), $p\text{-CMA-LGdH-1:1}$ (e). The d -values are given in nanometers.

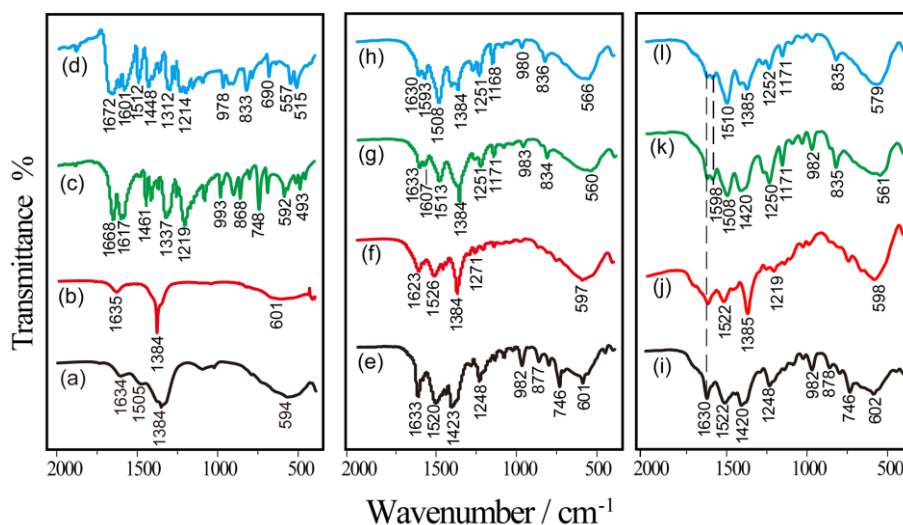


Fig. 2 FT-IR spectra of precursors $\text{NO}_3\text{-LEuH}$ (a), $\text{NO}_3\text{-LGdH}$ (b), $o\text{-CMA}$ (c), $p\text{-CMA}$ (d), and composites $o\text{-CMA-LEuH-1:1}$ (e), $o\text{-CMA-LEuH-1:2}$ (f), $p\text{-CMA-LEuH-1:1}$ (g), $p\text{-CMA-LEuH-1:1}$ (h), $o\text{-CMA-LGdH-1:1}$ (i), $o\text{-CMA-LGdH-1:2}$ (j), and $p\text{-CMA-LGdH-1:1}$ (k), $p\text{-CMA-LGdH-1:1}$ (l).

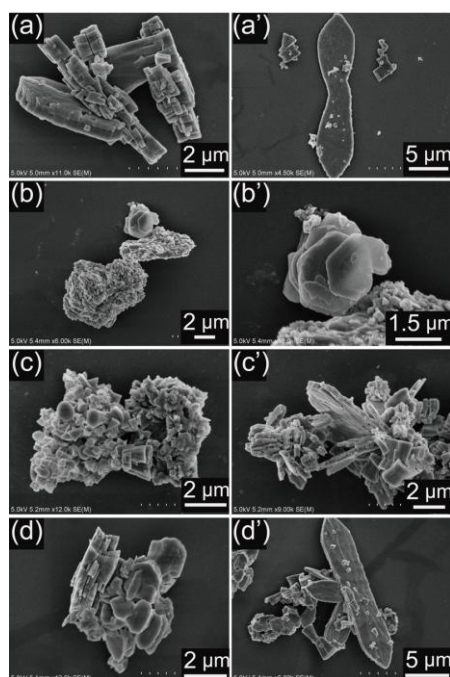


Fig. 3 SEM images of precursor $\text{NO}_3\text{-LEuH}$ (a, a'), and composites $o\text{-CMA-LEuH-1:1}$ (b, b'), $o\text{-CMA-LEuH-1:2}$ (c, c'), $p\text{-CMA-LEuH-1:1}$ (d, d'), $p\text{-CMA-LEuH-1:1}$ (e, e').

5

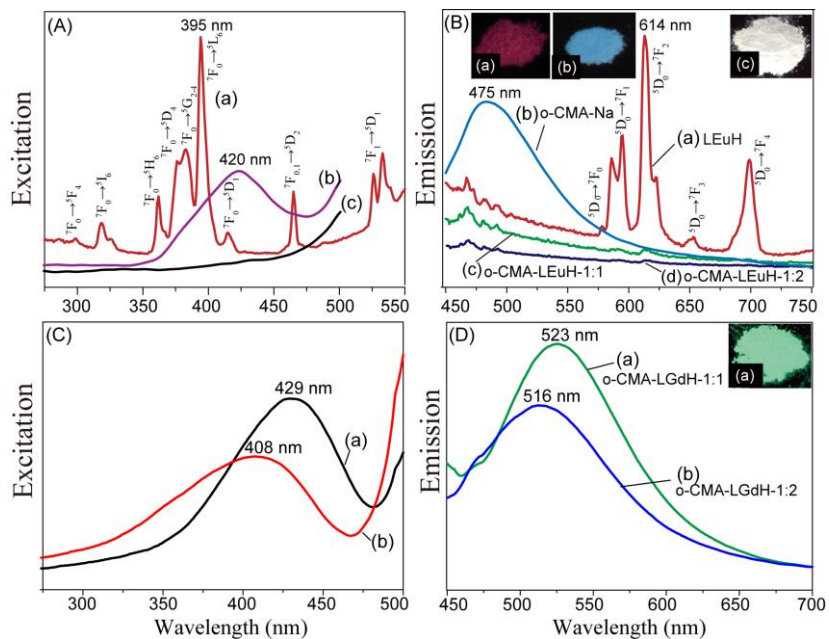


Fig. 4 (A) Powder excitation spectra of LEuH (a), $o\text{-CMA-Na}$ (b) $o\text{-CMA-LEuH-1:1}$ (c). (B) Powder emission spectra of LEuH (a), $o\text{-CMA-Na}$ (b) $o\text{-CMA-LEuH-1:1}$ (c) and $o\text{-CMA-LEuH-1:2}$ (d). (C) Powder excitation spectra of $o\text{-CMA-LGdH-1:1}$ (a), $o\text{-CMA-LGdH-1:2}$ (b). (D) Powder emission spectra of $o\text{-CMA-LGdH-1:1}$ (a), $o\text{-CMA-LGdH-1:2}$ (b). The insets are corresponding photographs under 365 nm UV irradiation.

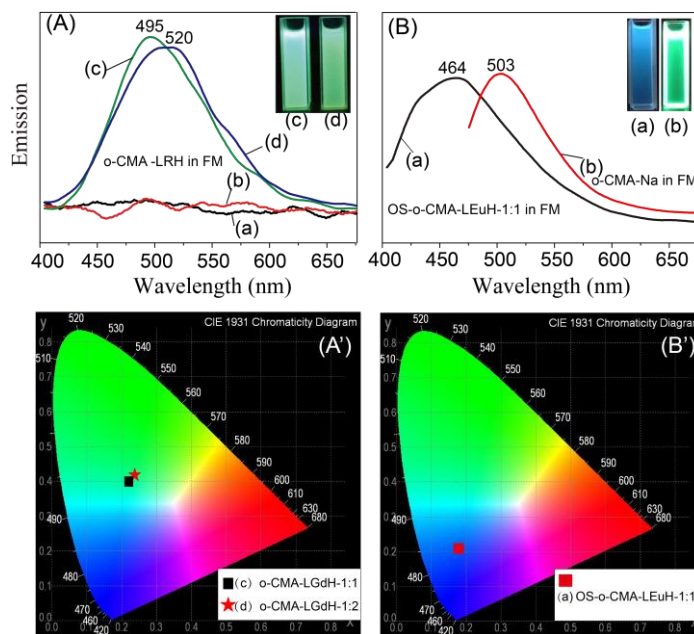


Fig. 5 (A) Emission spectra of *o*-CMA-LEuH composites in FM: *o*-CMA-LEuH-1:1 (a), *o*-CMA-LEuH-1:2 (b), *o*-CMA-LGdH-1:1 (c), *o*-CMA-LGdH-1:2 (d). (B) Emission spectra of OS-*o*-CMA-LEuH-1:1 composite (a) and *o*-CMA-Na in FM (b). (A') and (B') are CIE 1931 chromaticity diagrams of corresponding samples of (A) and (B) showing the photoluminescence color. The insets are corresponding photographs under 365 nm UV irradiation.

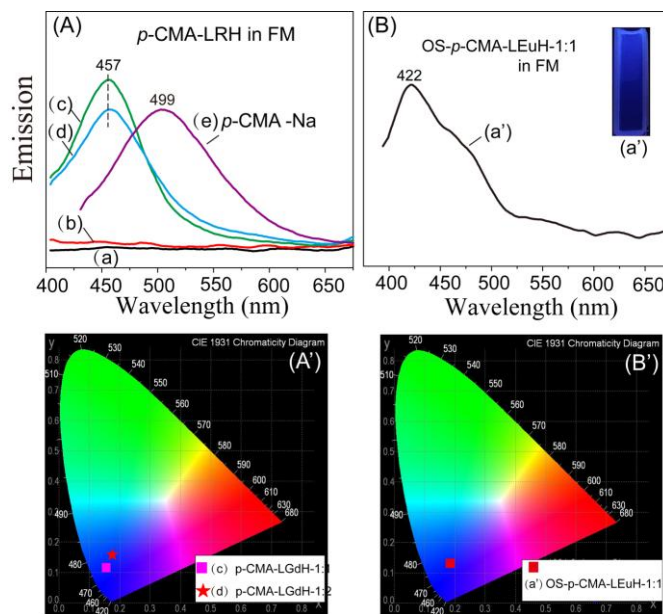
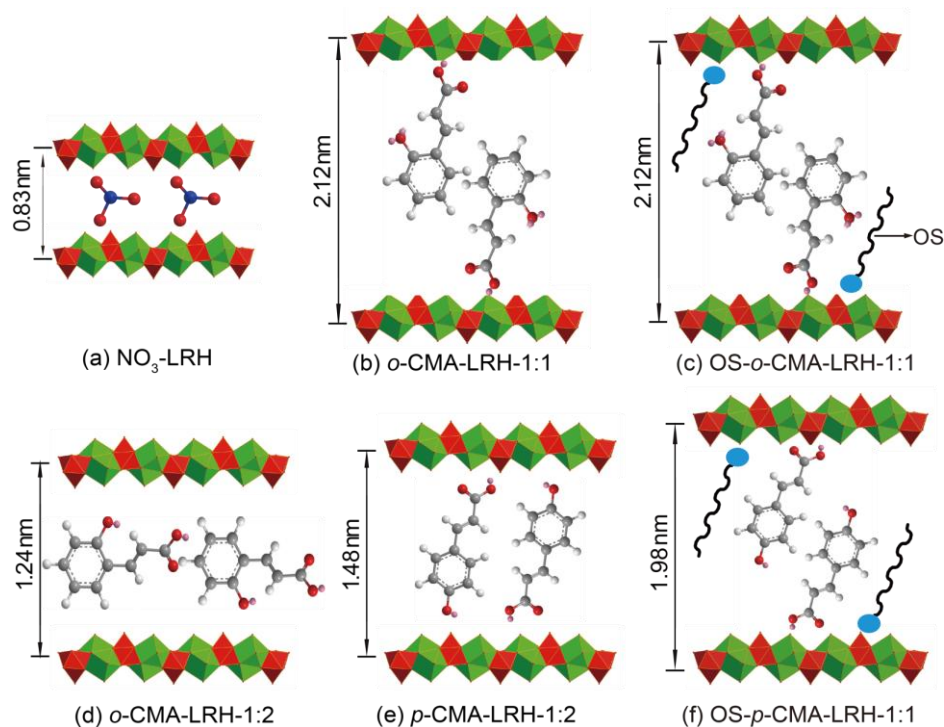
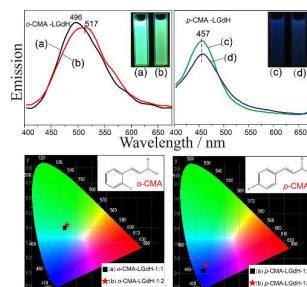


Fig. 6 (A) Emission spectra of samples in FM: *p*-CMA-LEuH-1:1 (a), *p*-CMA-LEuH-1:2 (b), *p*-CMA-LGdH-1:1 (c), *p*-CMA-LEuH-1:2 (d), and *p*-CMA-Na (e). (B) Emission spectra of OS-*p*-CMA-LEuH-1:1 (a'). (A') and (B') are CIE 1931 chromaticity diagrams of responding samples of (A) and (B) showing the photoluminescence color. The insets are corresponding photographs under 365 nm UV irradiation.



Scheme 1. Arrangements of gallery species in the composites: (a) NO_3 -LRH, (b) *o*-CMA-LRH-1:1, (c) OS-*o*-CMA-LRH-1:1, (d) *o*-CMA-LRH-1:2, (e) *p*-CMA-LRH-1:2, (f) OS-*p*-CMA-LRH-1:1.

Table of contents entry



Intercalation of two coumaric acids into LRHs forms composites which showed tunable luminescence depending on the state and layer ions.